

LEARNING A SPATIO-TEMPORAL EMBEDDING FOR VIDEO INSTANCE SEGMENTATION

Anthony Hu, Alex Kendall & Roberto Cipolla
University of Cambridge
{ah2029, agk34, rc10001}@cam.ac.uk

ABSTRACT

We present a novel embedding approach for video instance segmentation. Our method learns a spatio-temporal embedding integrating cues from appearance, motion, and geometry; a 3D causal convolutional network models motion, and a monocular self-supervised depth loss models geometry. In this embedding space, video-pixels of the same instance are clustered together while being separated from other instances, to naturally track instances over time without any complex post-processing. Our network runs in real-time as our architecture is entirely causal – we do not incorporate information from future frames, contrary to previous methods. We show that our model can accurately track and segment instances, even with occlusions and missed detections, advancing the state-of-the-art on the KITTI Multi-Object and Tracking Dataset.

1 INTRODUCTION

Explicitly predicting the motion of actors in a dynamic scene is a critical component of intelligent systems. Humans can seamlessly track moving objects in their environment by using cues such as appearance, relative distance, and most of all, temporal consistency: the world is rarely experienced in a static way: motion (or its absence) provides essential information to understand a scene. Similarly, incorporating past context through a temporal model is essential to segment and track objects consistently over time and through occlusions.

From a computer vision perspective, understanding object motion involves segmenting instances, estimating depth, and tracking instances over time. Instance segmentation has gained traction with challenging datasets such as COCO (Lin et al., 2014), Cityscapes (Cordts et al., 2016) and Mapillary Vistas (Neuhold et al., 2017). Such datasets, which only contain single-frame annotations, do not allow the training of video models with temporally consistent instance segmentation, nor does it allow self-supervised monocular depth estimation, that necessitates consecutive frames. Yet, navigating in the real-world requires temporally consistent segmentation and 3D geometry understanding of the other agents. More recently, a new dataset containing video instance segmentation annotations was



Figure 1: An illustration of our video instance segmentation model. Clockwise from top left: input image, predicted multi-object instance segmentation, visualisation of the high-dimensional embedding and predicted monocular depth.

released: the KITTI Multi-Object and Tracking Dataset (Voigtlaender et al., 2019). This dataset contains pixel-level instance segmentation on more than 8,000 video frames which effectively enables the training of video instance segmentation models.

In this work, we propose a new spatio-temporal embedding loss that learns to map video-pixels to a high-dimensional space¹. This space encourages video-pixels of the same instance to be close together and distinct from other instances. We show that this spatio-temporal embedding loss, jointly with a deep temporal convolutional neural network and self-supervised depth loss, produces consistent instance segmentations over time. The temporal model is a causal 3D convolutional network (only conditioned on past frames to predict the current embedding) and is capable of real-time operation. Finally, we show that predicting depth improves the quality of the embedding as the 3D geometry of an object constrains its future location given that objects move smoothly in space.

To summarise our novel contributions, we:

- introduce a new spatio-temporal embedding loss for video instance segmentation,
- show that having a temporal model improves embedding consistency over time,
- improve how the embedding disambiguates objects with a self-supervised monocular depth loss,
- handle occlusions, contrary to previous IoU based instance correspondence.

We demonstrate the efficacy of our method by advancing the state-of-the-art on the KITTI Multi-Object and Tracking Dataset (Voigtlaender et al., 2019). An example of our model’s output is given by Figure 1.

2 RELATED WORK

Two main approaches exist for single-image instance segmentation: region-proposal based (He et al., 2017; Hu et al., 2018; Chen et al., 2018; Liu et al., 2018) and embedding based (Brabandere et al., 2017; Fathi et al., 2017; Kong & Fowlkes, 2018; Kendall et al., 2018). The former method relies on a region of interest proposal network that first predicts bounding boxes then estimates the mask of the object inside that bounding box. With such a strategy, a given pixel could belong to the overlap of many bounding boxes, and it is largely unclear how correspondence between pixels can be learned. We instead favour the embedding based method and extend it to space and time.

Capturing the inter-relations of objects using multi-modal cues (appearance, motion, interaction) is difficult, as showcased by the Multi-Object Tracking (MOT) challenge (Xiang et al., 2015). Sadeghian et al. (2017) and Son et al. (2017) learned a representation of objects that follows the “tracking-by-detection” paradigm where the goal is to connect detections across video frames by finding the optimal assignment of a graph-based tracking formulation (i.e. each detection is a node, and an edge is the similarity score between two detections).

Collecting large-scale tracking datasets is necessary to train deep networks, but that process is expensive and time-consuming. Vondrick et al. (2018) introduced video colourisation as a self-supervised method to learn visual tracking. They constrained the colourisation problem of a grayscale image by learning to copy colours from a reference frame, with the pointing mechanism of the model acting as a tracker once it is fully trained. The colourisation model is more robust than optical flow based models, especially in complex natural scenes with fast motion, occlusion and dynamic backgrounds.

Voigtlaender et al. (2019) extended the task of multi-object tracking to multi-object tracking and segmentation (MOTS), by considering instance segmentations as opposed to 2D bounding boxes. Motivated by the saturation of the bounding box level tracking evaluations (Pont-Tuset et al., 2017), they introduced the KITTI MOTS dataset, which contains pixel-level instance segmentation on more than 8,000 video frames. They also trained a model which extends Mask R-CNN (He et al., 2017) by incorporating 3D convolutions to integrate temporal information, and the addition of an association head that produces an association vector for each detection, inspired from person re-identification (Beyer et al., 2017). The temporal component of their model, however, is fairly shallow (one or two layers), and is not causal, as future frames are used to segment past frames. More recently, Yang et al. (2019) collected a large-scale dataset from short YouTube videos (3-6 seconds) with video

¹See a [video demo](#) of our model.

instance segmentation labels, and Hu et al. (2019) introduced a densely annotated synthetic dataset with complex occlusions to learn how to estimate the spatial extent of objects beyond what is visible.

3 EMBEDDING-BASED VIDEO INSTANCE SEGMENTATION LOSS

Contrary to methods relying on region proposal (He et al., 2017; Chen et al., 2018), embedding-based instance segmentation methods map the pixels of a given instance to a structured high dimensional space, overcoming several limitations of region-proposal methods: (i) each pixel belongs to one unique instance (no bounding box overlap); (ii) the number of detected objects can be arbitrarily large (not fixed by the number of proposals).

We propose a spatio-temporal embedding loss with three competing forces, similarly to Brabandere et al. (2017). The attraction force (Equation (1)) encourages the video-pixels embedding of a given instance to be close to its embedding mean. The repulsion force (Equation (2)) incites the embedding mean of a given instance to be far from all others instances. And finally, the regularisation force (Equation (3)) prevents the embedding to diverge from the origin.

Let us denote by K the number of instances, and by S_k the set of all video-pixels of instance k . For all $i \in S_k$, we denote by y_i the embedding for pixel i and by μ_k the mean embedding of instance k : $\mu_k = \frac{1}{|S_k|} \sum_{i \in S_k} y_i$. The embedding loss is given by:

$$\mathcal{L}_a = \frac{1}{K} \sum_{k=1}^K \frac{1}{|S_k|} \sum_{i \in S_k} \max(0, \|\mu_k - y_i\|_2 - \rho_a)^2 \quad (1)$$

$$\mathcal{L}_r = \frac{1}{K(K-1)} \sum_{k_1 \neq k_2} \max(0, 2\rho_r - \|\mu_{k_1} - \mu_{k_2}\|_2)^2 \quad (2)$$

$$\mathcal{L}_{\text{reg}} = \frac{1}{K} \sum_{k=1}^K \|\mu_k\|_2 \quad (3)$$

ρ_a defines the attraction radius, constraining the embedding to be within ρ_a of its mean. ρ_r is the repulsion radius, constraining the mean embedding of two different instances to be at least $2\rho_r$ apart. Therefore, if we set $\rho_r > 2\rho_a$, a pixel embedding of an instance k will be closer to all the pixel embeddings $i \in S_k$ of instance k , than to the pixel embeddings of any other instance.

The spatio-temporal embedding loss is the weighted sum of the attraction, repulsion and regularisation forces:

$$\mathcal{L}_{\text{instance}} = \lambda_a \mathcal{L}_a + \lambda_r \mathcal{L}_r + \lambda_{\text{reg}} \mathcal{L}_{\text{reg}} \quad (4)$$

During inference, each pixel of the considered frame is assigned to an instance by randomly picking an unassigned pixel and aggregating close-by pixels with the mean shift algorithm (Comaniciu & Meer, 2002) until convergence. In the ideal case, with a test loss of zero, this will result in perfect instance segmentation.

3.1 SELF-SUPERVISED DEPTH ESTIMATION

The relative distance of objects is a strong cue for segmenting instances in video. Knowing the 3D geometry of objects especially helps segmenting instances in a temporally consistent way, as the past position of an instance effectively constrains where it could be next.

Depth estimation with supervised methods requires a vast quantity of high quality annotated data, which is challenging to acquire in a range of environments. As we have access to a video instance segmentation dataset, we can use a self-supervised depth loss from monocular video, where the supervision comes from consecutive frames.

Following Zhou et al. (2017) and Godard et al. (2019), we train a depth network with a separate pose estimation network with the hypothesis during training that scenes are mostly rigid, therefore

assuming appearance change is mostly due to camera motion. Pixels that violate this assumption are masked from the view synthesis loss, as they otherwise create infinite holes during inference for objects that are typically seen in motion during training – more details in Appendix A.1. The training signal comes from novel view synthesis, i.e. the generation of a new image of the scene from a different camera pose. Let us denote by (I_1, I_2, \dots, I_T) a sequence of images, I_t the target view and I_s the source view. The view synthesis loss is given by:

$$\mathcal{L}_{vs} = \sum_{s \neq t} e(I_t, \hat{I}_{s \rightarrow t}) \quad (5)$$

with $\hat{I}_{s \rightarrow t}$ the synthesised view of I_t , from source image I_s and using the predicted depth \hat{D}_t and the estimated camera transformation $\hat{T}_{t \rightarrow s}$. The projection error e is a weighted sum of an L_1 distance, a Structural Similarity Index (SSIM) and a smoothness regularisation term, as in Zhao et al. (2017). Let us denote by p_t the coordinate of a pixel in the target image I_t in homogeneous coordinates. Given the camera intrinsic matrix, K , and the mapping φ from image plane to camera coordinate, the corresponding pixel in the source image is provided by:

$$p_s \sim K \hat{T}_{t \rightarrow s} \varphi(K^{-1} p_t, \hat{D}_t(p_t)) \quad (6)$$

Since the projected coordinates p_s take continuous values, we use the Spatial Transformer Network (Jaderberg et al., 2015) sampling mechanism to bilinearly interpolate the four neighbouring pixels to populate the reconstructed image $\hat{I}_{s \rightarrow t}$.

Some pixels are visible in the target image, but are not in the source image, leading to a large projection error. As advocated by Godard et al. (2019), instead of summing, taking the minimum projection error greatly reduces artifacts due to occlusion and results in sharper predictions. The resulting view synthesis loss is:

$$\mathcal{L}_{vs} = \min_{s \neq t} e(I_t, \hat{I}_{s \rightarrow t}) \quad (7)$$

The final video instance embedding loss is the weighted sum of the attraction, repulsion, regularisation and geometric view synthesis losses:

$$\mathcal{L}_{\text{embedding}} = \lambda_a \mathcal{L}_a + \lambda_r \mathcal{L}_r + \lambda_{\text{reg}} \mathcal{L}_{\text{reg}} + \lambda_{vs} \mathcal{L}_{vs} \quad (8)$$

4 MODEL ARCHITECTURE

Our network contains three components: the encoder, the temporal model and the decoders. Each input frame I_t is first encoded as a compact feature x_t , then the temporal model learns a rich spatio-temporal representation z_t , and finally, the decoders output the instance embedding and depth prediction as illustrated by Figure 2.

Encoder. We use a ResNet-18 (He et al., 2016) as our encoder, which allows the network to run in real-time on sequences of images.

Temporal Model. The model learns scene dynamics with a causal 3D convolutional network made of 3D residual convolutional blocks (convolving in both space and time, with residual connections). For a given time index, t , the network only convolves over images from indices $s \leq t$ to compute the temporal representation z_t . It therefore does not use future frames and is completely causal. The temporal model does not decimate the spatial dimension of the encoding, but slowly accumulates information over time from the previous encodings x_s with $s \leq t$. It is trained efficiently with convolutions as all input images are available during training, enabling parallel computations with GPUs. However, during inference, the model is inherently sequential, but can be made significantly faster by caching the convolutional features over time and eliminating redundant operations, as proposed by Paine et al. (2016) for WaveNet (Oord et al., 2016).

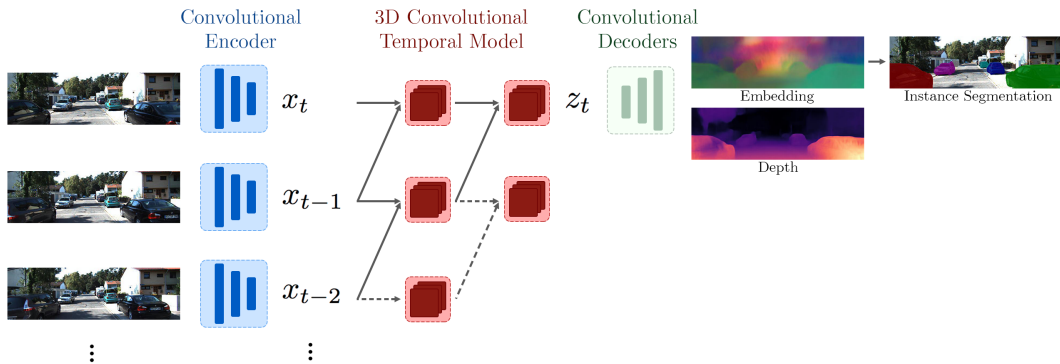


Figure 2: Our spatio-temporal embedding network. The representation z_t is trained to encode appearance, motion and geometry cues in order to predict instance embedding and monocular depth.

Decoders. From the temporal representation z_t , the decoders output the instance embedding $y_t \in \mathbb{R}^{p \times H \times W}$ and estimated depth $\hat{D}_t \in \mathbb{R}^{1 \times H \times W}$, with p the embedding dimension and (H, W) the input image size.

Pose and Mask Model. The architecture of the Pose and Mask networks are given in Appendix A.1.

4.1 INFERENCE

For each new frame, we first mask the background with our mask network, then we cluster the foreground embeddings with mean shift to discover dense regions with each cluster corresponding to one instance. Tracking instances simply requires comparing the mean embedding of a newly segmented instance with previously segmented instances. A distance lower than ρ_r indicates a match.

The embeddings are accumulated over time, creating increasingly denser regions over time and resulting in a better clustering. To ensure that the pixel embeddings of a particular instance can smoothly vary over time, the embeddings have a life span corresponding to the time sequence length of the embedding loss.

5 EXPERIMENTS

Next we describe experimental evidence which demonstrates the performance of our method by advancing the state-of-the-art on the KITTI Multi-Object and Tracking Dataset (Voigtlaender et al., 2019).

5.1 DATASET

The KITTI Multi-Object Tracking and Segmentation (MOTS) dataset contains 8,008 frames with instance segmentation labels resulting in a total of 26,899 annotated cars (see Table 1). It is composed of 21 scenes with a resolution of 375×1242 with consistent instance ID labels across time, allowing the training of video instance segmentation models. The frames are annotated at 10 frames per second, which is suitable for self-supervised monocular depth prediction.

	Scenes	Frames	Annotations	Avg. # frames	Avg. # annotations
Train	12	5,027	18,831	419	1,569
Validation	9	2,981	8,068	331	896

Table 1: Details of the KITTI Multi-Object Tracking and Segmentation (MOTS) dataset.

The ApolloScape dataset (Huang et al., 2018) also contains video instance segmentation labels for 49,287 frames, but the annotations are not consistent in time, rendering the training of a temporal model impossible. NuScenes (Caesar et al., 2019) features 1,000 scenes of 20 seconds with annotations at 2Hz in a diverse range of environments (different weather, daytime, city) but only contains bounding box labels, failing to represent the fine-grained details of instance segmentation. Temporal instance segmentation is also available on short snippets of the DAVIS dataset (Pont-Tuset et al., 2017), but each snippet is recorded by a different camera and is too short to effectively learn a depth model. For this reason, we focus on the KITTI MOTS dataset – it is the only dataset that contains consistent video instance segmentation in a sufficient quantity to train deep models.

5.2 HYPER-PARAMETERS

We halve the input images to our encoder to use an input RGB resolution of 192×640 . The spatio-temporal representation $z_t \in \mathbb{R}^{128 \times 24 \times 80}$ and the embedding dimension is $p = 8$. Except for the experiments in Table 4, we train with a sequence length of 5 which corresponds to 0.5 seconds of temporal context since the videos are 10Hz.

In the loss function, we set the attraction radius $\rho_a = 0.5$ and repulsion radius $\rho_r = 1.5$. We weight the losses with attraction and repulsion loss weight $\lambda_a = \lambda_r = 1.0$, regularisation loss $\lambda_{\text{reg}} = 0.001$ and depth loss $\lambda_{vs} = 1.0$.

5.3 METRICS

In this section, we define multi-object tracking and segmentation metrics, measuring the quality of the segmentation as well as the consistency of the predictions over time. Let us denote by \mathbb{H} the set of predicted ids, \mathbb{G} the set of ground truth ids and ψ the mapping from hypothesis segmentations to ground truth segmentations. $\psi : \mathbb{H} \rightarrow \mathbb{G} \cup \emptyset$ is defined as:

$$\psi(h) = \begin{cases} \operatorname{argmax}_g \operatorname{IoU}(h, g), & \text{if } \max_g \operatorname{IoU}(h, g) > \text{threshold} \\ \emptyset, & \text{otherwise} \end{cases} \quad (9)$$

We further define the following sets: TP (true positives), FP (false positives), FN (false negatives), IDS (the set of ID switches), and \tilde{TP} the soft number of true positives: $\tilde{TP} = \sum_{h \in TP} \operatorname{IoU}(h, \psi(h))$.

Following Voigtlaender et al. (2019), we define the following MOTS metrics: multi-object tracking and segmentation precision (MOTSP), multi-object tracking and segmentation accuracy (MOTSA) and finally the soft multi-object tracking and segmentation accuracy (sMOTSA) that measures segmentation as well as detection and tracking quality.

$$\text{MOTSP} = \frac{|\tilde{TP}|}{|TP|} \quad (10)$$

$$\text{MOTSA} = 1 - \frac{|FP| + |FN| + |IDS|}{|\mathbb{M}|} = \frac{|TP| - |FP| - |IDS|}{|\mathbb{M}|} \quad (11)$$

$$\text{sMOTSA} = \frac{|\tilde{TP}| - |FP| - |IDS|}{|\mathbb{M}|} \quad (12)$$

5.4 RESULTS

We compare our model to the following baselines for video instance segmentation and report the results in Table 2.

- **Single-frame embedding loss** (Brabandere et al., 2017), previous state-of-the-art method where instance segmentations are propagated in time using intersection-over-union association.
- **Mask R-CNN** (He et al., 2017), instances are propagated with intersection-over-union.
- **Without temporal model**, spatio-temporal embedding loss, without the temporal model.

- **Without depth**, temporal model and spatio-temporal embedding loss, without the depth loss.

	MOTSA	sMOTSA	MOTSP	AP
Brabandere et al. (2017)	0.575	0.423	0.803	0.612
Mask R-CNN	0.584	0.455	0.833	0.646
Without temporal model	0.582	0.426	0.799	0.607
Without depth	0.591	0.433	0.801	0.614
Ours	0.613	0.461	0.801	0.600

Table 2: KITTI MOTS validation set results comparing our model with baseline approaches.

The static detection metrics (MOTSP and average precision) are evaluated image by image without taking into account the temporal consistency of the instance segmentations. As the compared models (Without temporal model, Without depth, Ours) are all using the same mask network, they show similar performance in terms of detection. However, when evaluating performance on metrics that measures temporal consistency (MOTSA and sMOTSA), our best model shows significant improvement over the baselines.

The variant without the temporal model performs poorly as it does not have any temporal context to learn a spatio-temporal embedding and therefore only relies on spatial appearance. The temporal model on the other hand learns with the temporal context and local motion, which results in a better embedding. Our model, which learns to predict both a spatio-temporal embedding and monocular depth, achieves the best performance. In addition to using cues from appearance and temporal context, estimating depth allows the network to use information from the relative distance of objects to disambiguate them. Finally, we observe that our model outperforms Mask R-CNN (He et al., 2017) on the temporal metrics (MOTSA and sMOTSA) even though the latter exhibits a higher detection accuracy, further demonstrating the temporal consistency quality of our spatio-temporal embedding.

5.4.1 ANALYSIS OF CLUSTERING AND BACKGROUND SEGMENTATION.

Our model relies on segmenting the background to determine the pixel locations to consider for instance clustering when applying mean shift. We evaluate the impact of using the ground truth mask against our predicted mask in Table 3. The performance gain is significant, hinting that our model could be improved with a more powerful mask network.

Next, we evaluate the effect of clustering. In the best scenario, the validation loss would be zero, and the clustering would be perfect using the mean shift algorithm. However, this scenario is unlikely and the clustering algorithm is affected by noisy embeddings. We evaluate the effect of this noise by clustering with the ground-truth mean: we threshold with a radius ρ_r around the ground truth instance embedding mean. This also results in a boost in the evaluation metrics, but most interestingly, a model that uses both ground truth instance embedding mean clustering and ground truth mask performs worse than a model using the ground truth mask and our clustering algorithm. This is because our clustering algorithm accumulates embeddings from past frames and therefore creates an attraction force for the mean shift algorithm that enables the instances to be matched more consistently.

GT Mean	GT Mask	MOTSA	sMOTSA	MOTSP	AP
\times	\times	0.613	0.461	0.801	0.600
\checkmark	\times	0.700	0.616	0.897	0.691
\times	\checkmark	0.804	0.751	0.936	0.786
\checkmark	\checkmark	0.714	0.644	0.915	0.710

Table 3: Comparing the effect of noisy against ground-truth clustering and background segmentation on the KITTI MOTS dataset.

5.4.2 EFFECT OF THE SEQUENCE LENGTH

Our model learns a spatio-temporal embedding that enables clustering the video-pixels of each instance. Instance correspondence between frames is achieved by matching newly detected instances to previous instances if the mean embedding distance is below the repulsion radius, p_r . Therefore, We can track instances for an arbitrarily long period of time, as long as the embedding of a given instance changes smoothly over time, which is likely the case as temporal context and depth evolve progressively.

However, when the network is trained over sequence of images which are too long, the learning process of the embedding collapses. This is because the attractive loss term is detrimental between distant frames as it pressures pixels from the same instance to have corresponding embeddings when their appearance and depth is no longer similar. It also suggests our model is able to reason over lower order motion cues more effectively than longer term dynamics. This is seen experimentally in Table 4.

Length	1	3	5	7	10	15
MOTSA	0.575	0.590	0.613	0.555	0.538	0.402
sMOTSA	0.423	0.435	0.461	0.402	0.398	0.273
MOTSP	0.803	0.810	0.801	0.788	0.792	0.783

Table 4: Influence of the sequence length on model performance. This indicates that our model can learn short-term motion features effectively, but not long-term cues. We reason that this is because over longer sequences, the loss prevents the embedding smoothly shifting, which naturally occurs to changing pose, appearance, context and lighting in the scene. We find the optimum sequence length on this dataset to be five.

5.5 QUALITATIVE EXAMPLES

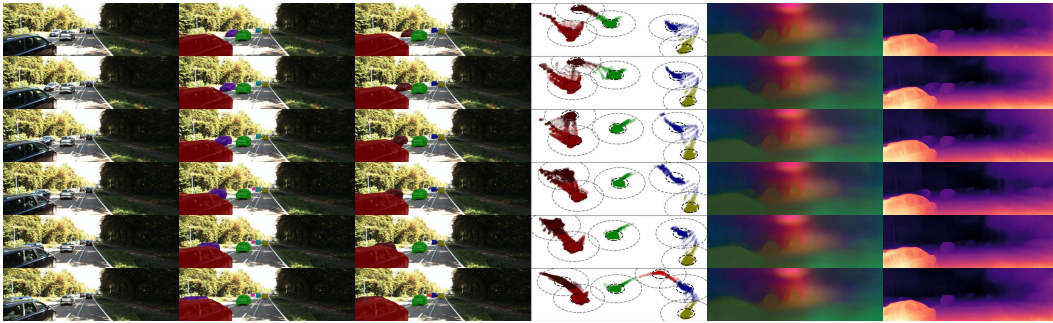
We show that our model can consistently segment instances over time on the following challenging scenarios: tracking through partial (Figure 3a) and full occlusion (Figure 3c), and continuous tracking through noisy detections (Figure 3b). Additional examples and failure cases of our model are shown in Appendix A.2 and in our [video demo](#).

In each example, we show from left to right: RGB input image, ground truth instance segmentation, predicted instance segmentation, embedding visualised in 2D, embedding visualised in RGB and predicted monocular depth. The embedding is visualised in 2D and coloured with the results of the mean shift clustering. Each colour represents a different instance, the inner circle indicates the attraction radius from the instance mean embedding, and the outer circle represents the repulsion radius of each instance. Additionally, we also visualise the embedding spatially in 3D, by projecting its three principal components to an RGB image.

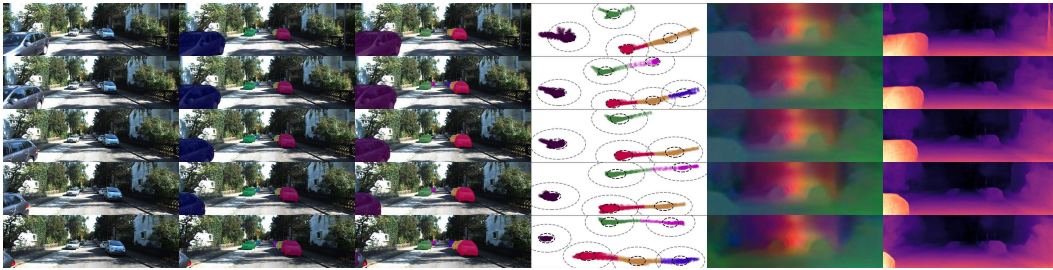
Finally, we show in Appendix A.2 that incorporating depth context greatly improves the quality of the embedding, especially in complex scenarios such as partial or total occlusion. We also observe that the embedding is much more structured when using depth, further validating that 3D geometry is essential to reason about dynamics agents in video.

6 CONCLUSIONS

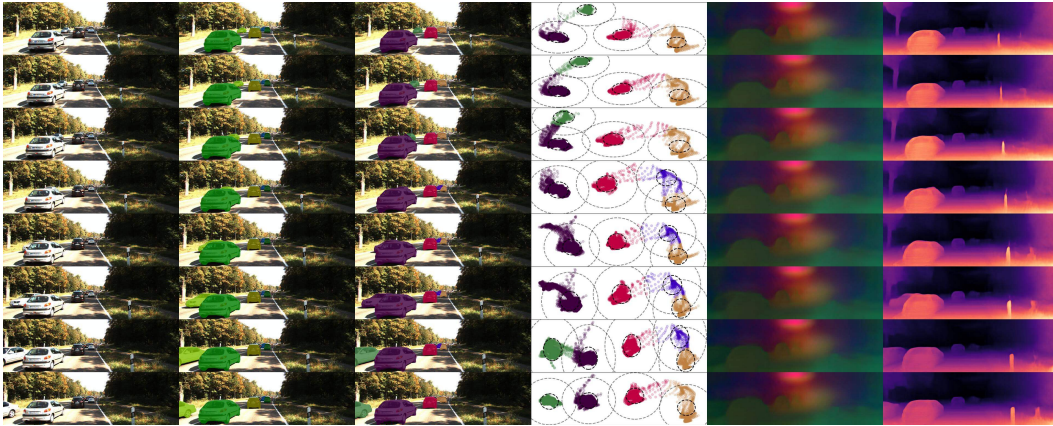
We presented a new spatio-temporal embedding loss that generates consistent instance segmentation over time. The temporal network models the past temporal context and the depth network constrains the embedding to aid disambiguation between objects. We demonstrated that our model could effectively track occluded instances or instances with missed detections, by leveraging the temporal and depth context. Our method advanced the state-of-the-art at video instance segmentation on the KITTI Multi-Object and Tracking Dataset.



(a) **Partial occlusion.** The brown car is correctly segmented even when being partially occluded by the red car, as the embedding contains past temporal context and is aware of the motion of the brown car.



(b) **Continuous tracking.** The segmented pink and purple cars are accurately tracked even with missing detections.



(c) **Total occlusion.** The green car is correctly tracked, even though it was completely occluded by another car.

Figure 3: From left to right: RGB input image, ground truth instance segmentation, predicted instance segmentation, embedding visualised in 2D, embedding visualised in RGB and predicted monocular depth.

REFERENCES

- Lucas Beyer, Stefan Breuers, Vitaly Kurin, and Bastian Leibe. Towards a principled integration of multi-camera re-identification and tracking through optimal bayes filters. In *arXiv:1705.04608*, 2017.
- Bert De Brabandere, Davy Neven, and Luc Van Gool. Semantic instance segmentation with a discriminative loss function. *CVPRw*, abs/1708.02551, 2017.
- Holger Caesar, Varun Bankiti, Alex H. Lang, Sourabh Vora, Venice Erin Liong, Qiang Xu, Anush Krishnan, Yu Pan, Giancarlo Baldan, and Oscar Beijbom. nuscenes: A multimodal dataset for autonomous driving. *arXiv preprint arXiv:1903.11027*, 2019.
- Liang-Chieh Chen, Alexander Hermans, George Papandreou, Florian Schroff, Peng Wang, and Hartwig Adam. Masklab: Instance segmentation by refining object detection with semantic and direction features. *2018 IEEE/CVF Conference on Computer Vision and Pattern Recognition*, 2018.
- Dorin Comaniciu and Peter Meer. Mean shift: A robust approach toward feature space analysis. *IEEE Transactions on Pattern Analysis & Machine Intelligence*, pp. 603–619, 2002.
- Marius Cordts, Mohamed Omran, Sebastian Ramos, Timo Rehfeld, Markus Enzweiler, Rodrigo Benenson, Uwe Franke, Stefan Roth, and Bernt Schiele. The cityscapes dataset for semantic urban scene understanding. In *Proc. of the IEEE Conference on Computer Vision and Pattern Recognition (CVPR)*, 2016.
- Alireza Fathi, Zbigniew Wojna, Vivek Rathod, Peng Wang, Hyun Oh Song, Sergio Guadarrama, and Kevin P. Murphy. Semantic instance segmentation via deep metric learning. *ArXiv*, abs/1703.10277, 2017.
- Clément Godard, Oisin Mac Aodha, Michael Firman, and Gabriel J. Brostow. Digging into self-supervised monocular depth prediction. *The International Conference on Computer Vision (ICCV)*, October 2019.
- Kaiming He, Xiangyu Zhang, Shaoqing Ren, and Jian Sun. Deep residual learning for image recognition. In *CVPR*, 2016.
- Kaiming He, Georgia Gkioxari, Piotr Dollar, and Ross Girshick. Mask R-CNN. In *Proceedings of the International Conference on Computer Vision (ICCV)*, 2017.
- Yuan-Ting Hu, Jia-Bin Huang, and Alexander G. Schwing. Maskrnn: Instance level video object segmentation. *NIPS*, abs/1803.11187, 2018.
- Yuan-Ting Hu, Hong-Shuo Chen, Kexin Hui, Jia-Bin Huang, and Alexander G. Schwing. Sail-vos: Semantic amodal instance level video object segmentation - a synthetic dataset and baselines. In *CVPR*, 2019.
- Xinyu Huang, Xinjing Cheng, Qichuan Geng, Binbin Cao, Dingfu Zhou, Peng Wang, Yuanqing Lin, and Ruigang Yang. The apollo-scape dataset for autonomous driving. In *The IEEE Conference on Computer Vision and Pattern Recognition (CVPR) Workshops*, June 2018.
- Max Jaderberg, Karen Simonyan, Andrew Zisserman, and Koray Kavukcuoglu. Spatial transformer networks. In *Proceedings of the 28th International Conference on Neural Information Processing Systems - Volume 2*, NIPS’15, pp. 2017–2025, Cambridge, MA, USA, 2015. MIT Press.
- Alex Kendall, Yarin Gal, and Roberto Cipolla. Multi-task learning using uncertainty to weigh losses for scene geometry and semantics. In *Proceedings of the IEEE Conference on Computer Vision and Pattern Recognition (CVPR)*, 2018.
- Shu Kong and Charless Fowlkes. Recurrent pixel embedding for instance grouping. In *2018 Conference on Computer Vision and Pattern Recognition (CVPR)*, 2018.
- Tsung-Yi Lin, Michael Maire, Serge J. Belongie, Lubomir D. Bourdev, Ross B. Girshick, James Hays, Pietro Perona, Deva Ramanan, Piotr Dollár, and C. Lawrence Zitnick. Microsoft coco: Common objects in context. In *ECCV*, 2014.

-
- Shu Liu, Lu Qi, Haifang Qin, Jianping Shi, and Jiaya Jia. Path aggregation network for instance segmentation. *2018 IEEE/CVF Conference on Computer Vision and Pattern Recognition*, pp. 8759–8768, 2018.
- Gerhard Neuhold, Tobias Ollmann, Samuel Rota Bulò, and Peter Kotschieder. The mapillary vistas dataset for semantic understanding of street scenes. In *International Conference on Computer Vision (ICCV)*, 2017.
- Aaron van den Oord, Sander Dieleman, Heiga Zen, Karen Simonyan, Oriol Vinyals, Alex Graves, Nal Kalchbrenner, Andrew Senior, and Koray Kavukcuoglu. Wavenet: A generative model for raw audio, 2016.
- Tom Le Paine, Pooya Khorrani, Shiyu Chang, Yang Zhang, Prajit Ramachandran, Mark A Hasegawa-Johnson, and Thomas S Huang. Fast wavenet generation algorithm. *arXiv preprint arXiv:1611.09482*, 2016.
- J. Pont-Tuset, F. Perazzi, S. Caelles, P. Arbelaez, A. Sorkine-Hornung, and L. Van Gool. The 2017 davis challenge on video object segmentation. *arXiv:1704.00675*, 2017.
- Amir Sadeghian, Alexandre Alahi, and Silvio Savarese. Tracking the untrackable: Learning to track multiple cues with long-term dependencies. In *ICCV*, 2017.
- Jeany Son, Mooyeol Baek, Minsu Cho, and Bohyung Han. Multi-object tracking with quadruplet convolutional neural networks. *2017 IEEE Conference on Computer Vision and Pattern Recognition (CVPR)*, pp. 3786–3795, 2017.
- Paul Voigtlaender, Michael Krause, Aljosa Osep, Jonathon Luiten, Berin Balachandar Gnana Sekar, Andreas Geiger, and Bastian Leibe. Mots: Multi-object tracking and segmentation. In *Proceedings IEEE Conf. on Computer Vision and Pattern Recognition (CVPR)*, 2019.
- Carl Martin Vondrick, Abhinav Shrivastava, Alireza Fathi, Sergio Guadarrama, and Kevin Murphy. Tracking emerges by coloring videos. In *ECCV*, 2018.
- Yu Xiang, Alexandre Alahi, and Silvio Savarese. Learning to track: Online multi-object tracking by decision making. In *International Conference on Computer Vision*, 2015.
- Linjie Yang, Yuchen Fan, and Ning Xu. Video instance segmentation. *ICCV*, 2019.
- Hang Zhao, Orazio Gallo, Iuri Frosio, and Jan Kautz. Loss functions for image restoration with neural networks. *IEEE Transactions on Computational Imaging*, 3:47–57, 2017.
- Tinghui Zhou, Matthew Brown, Noah Snavely, and David Lowe. Unsupervised learning of depth and ego-motion from video. In *Computer Vision and Pattern Recognition*, 2017.

A APPENDIX

A.1 NETWORK ARCHITECTURE DETAILS

We report the details of each component of our model in this section. The number of parameters and layers of each module are in Table 5.

	Encoder	Temporal	Decoders	Pose	Mask
Parameters	14.6M	0.7M	0.4M	13.0M	14.8M
Layers	18	36	7	22	25

Table 5: Number of parameters and layers of each module.

Encoder. The encoder is a ResNet-18 convolutional layer (He et al., 2016), with 128 output channels.

Temporal model. The temporal model contains 12 residual 3D convolutional blocks. Each residual block is the succession of: a 3D projection convolution with kernel size $1 \times 1 \times 1$ to halve the number of channels, a 3D causal convolutional layer with kernel $t \times 3 \times 3$, and a 3D projection convolution with kernel $1 \times 1 \times 1$ to restore the number of channels.

We set the temporal kernel size to $t = 2$, and the number of output channels to 128.

Decoders. The decoders for instance embedding and depth estimation are identical and consist of 7 convolutional layers with channels [64, 64, 32, 32, 16, 16] and 3 upsampling layers. The final convolutional layer contains $p = 8$ channels for instance embedding and 1 channel for depth.

Depth Masking. During training, we remove from the photometric reprojection loss the pixels that violate the rigid scene assumption, i.e. the pixels whose appearance do not change between adjacent frames. We set the mask M to only include pixels where the reprojection error is lower with the warped image $\hat{I}_{s \rightarrow t}$ than the unwarped source image I_s :

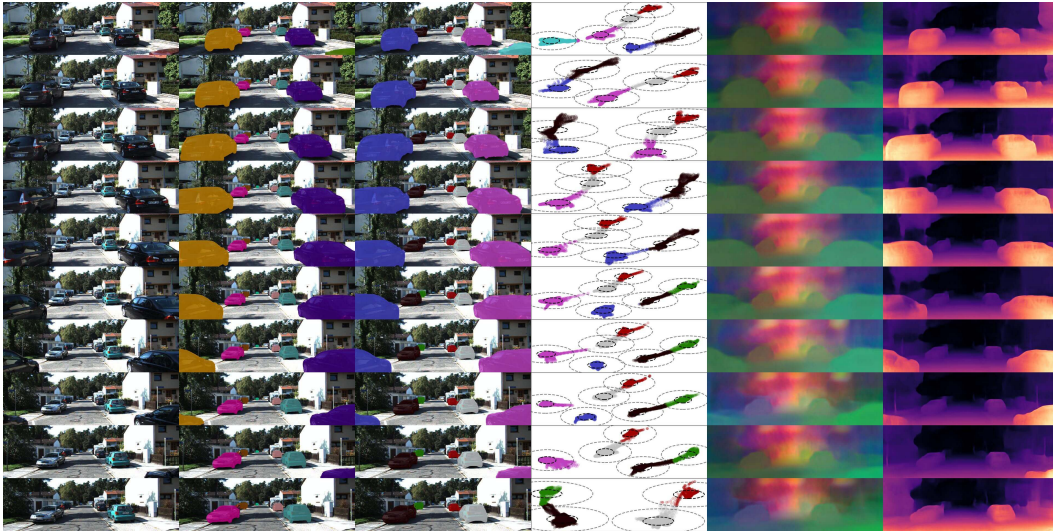
$$M = \left[\min_s e(I_t, \hat{I}_{s \rightarrow t}) < \min_s e(I_t, I_s) \right]$$

Pose Network. The pose network is the succession of a ResNet-18 model followed by 4 convolutions with [256, 256, 256, 6] channels. The last feature map is averaged to output a single 6-DoF transformation matrix.

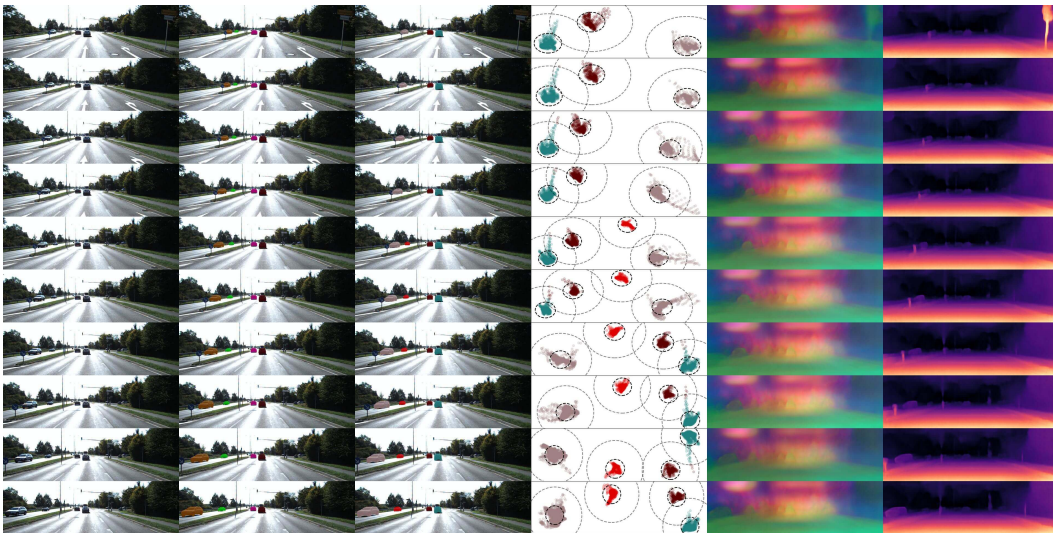
Mask Network. The mask network is trained separately to mask the background and is the succession of the Encoder and Decoder described above.

A.2 ADDITIONAL QUALITATIVE EXAMPLES

The following examples show qualitative results and failure examples of our video instance segmentation model on the KITTI Multi-Object and Tracking Dataset. From left to right: RGB input image, ground truth instance segmentation, predicted instance segmentation, embedding visualised in 2D, embedding visualised in RGB and predicted monocular depth.

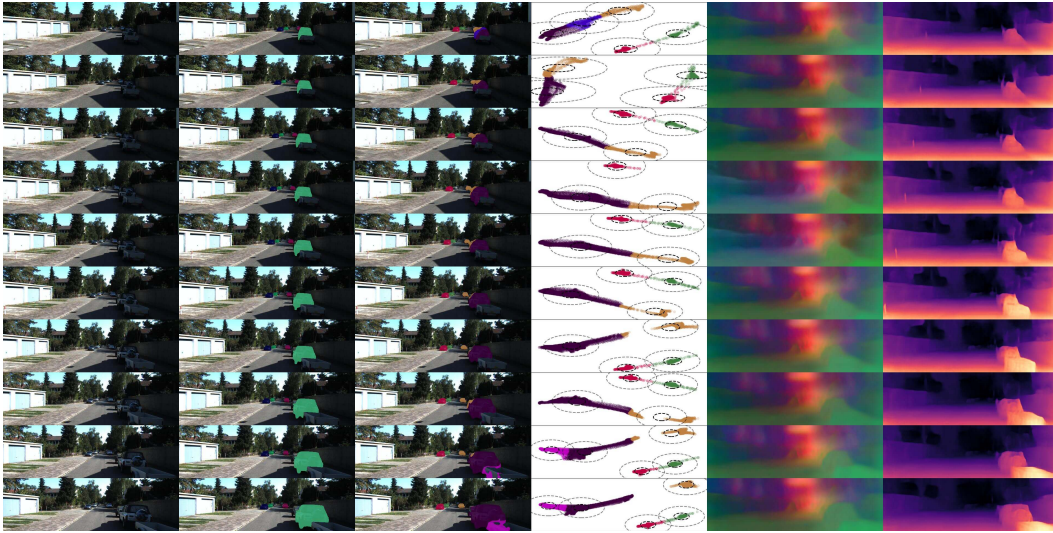


(a) Video instance segmentation of parked cars.

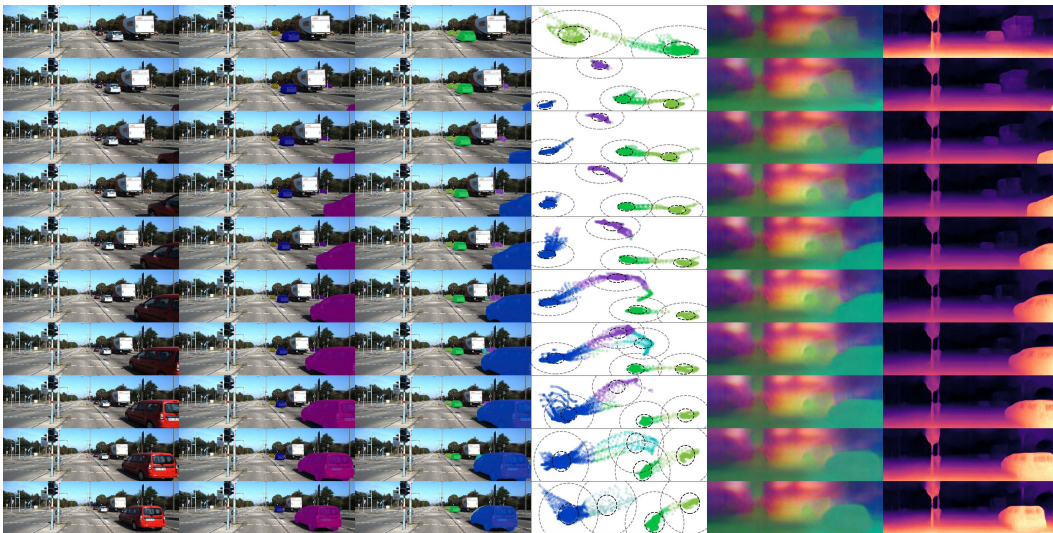


(b) Video instance segmentation of other traffic.

Figure 4: From left to right: RGB input image, ground truth instance segmentation, predicted instance segmentation, embedding visualised in 2D, embedding visualised in RGB and predicted monocular depth.



(a) Failure case: the vehicle is segmented into two separate instances.

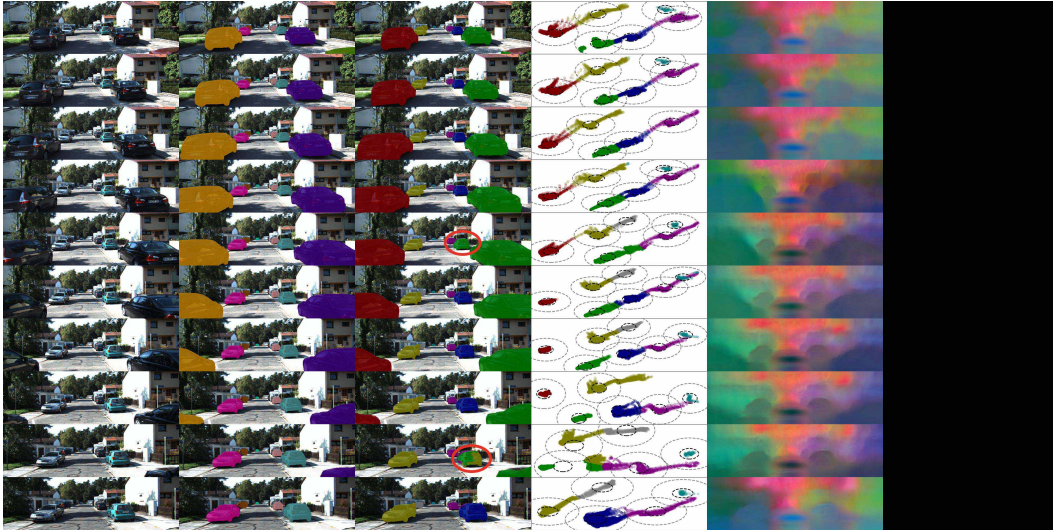


(b) Failure case: two far-away cars are segmented as one instance.

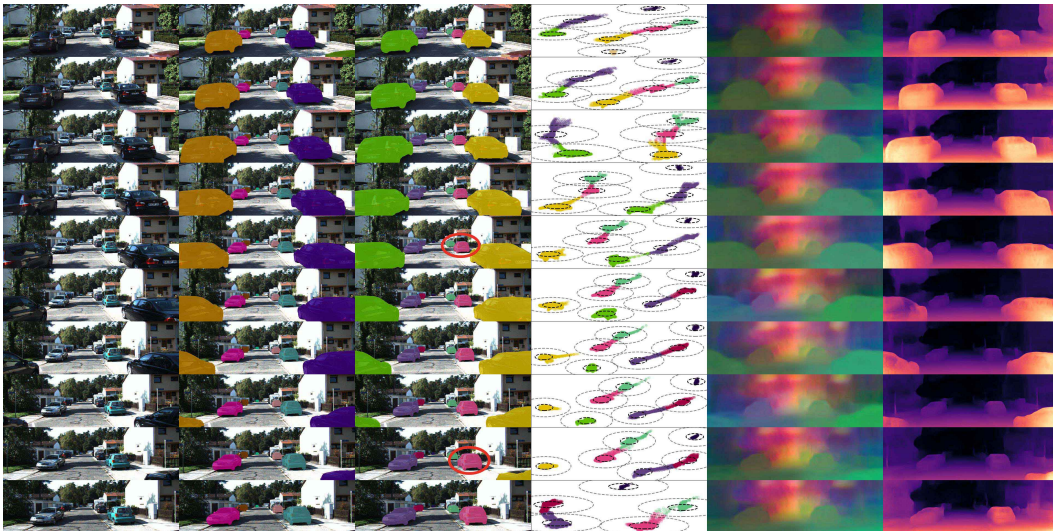
Figure 5: From left to right: RGB input image, ground truth instance segmentation, predicted instance segmentation, embedding visualised in 2D, embedding visualised in RGB and predicted monocular depth.

A.3 QUALITATIVE IMPROVEMENTS WITH DEPTH

We show that our model greatly benefits from depth estimation, with the learned embedding being more structured, and correctly tracking objects in difficult scenarios such as partial or total occlusion.

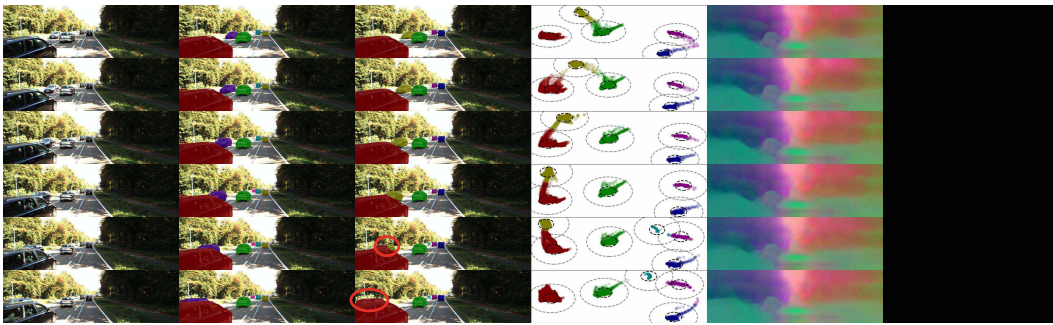


(a) Without depth estimation.

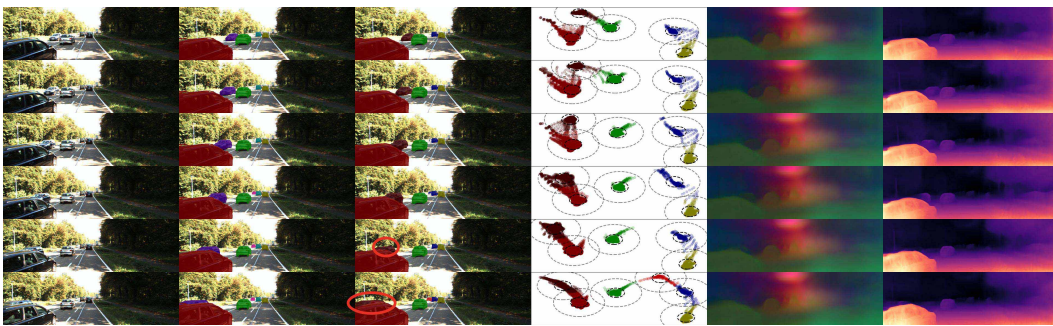


(b) With depth estimation

Figure 6: From left to right: RGB input image, ground truth instance segmentation, predicted instance segmentation, embedding visualised in 2D, embedding visualised in RGB and predicted monocular depth. Without depth estimation, the car circled in red is wrongly tracked in frame 5 and 9, while the model with depth correctly tracks it as the network has learned a consistent embedding based not only on appearance, but also on 3D geometry. Also, the RGB projection of the embedding from our model is considerably better and much more structured.

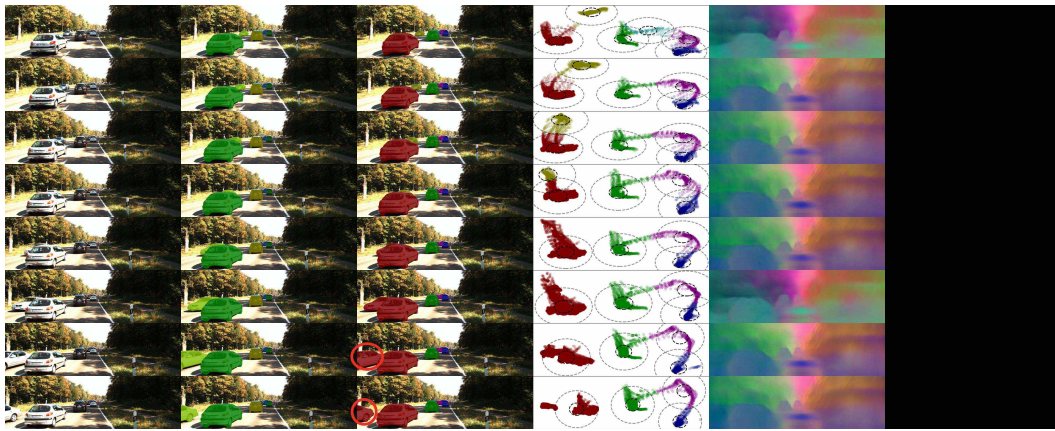


(a) Without depth estimation.

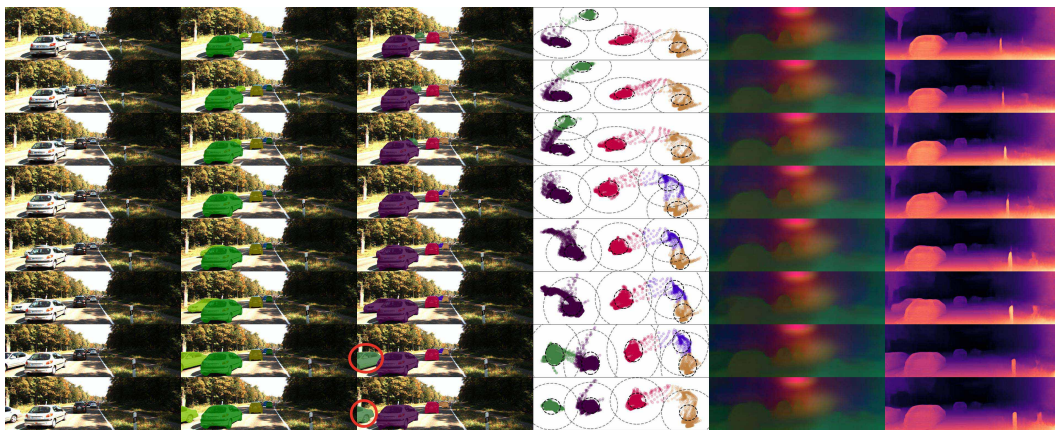


(b) With depth estimation

Figure 7: From left to right: RGB input image, ground truth instance segmentation, predicted instance segmentation, embedding visualised in 2D, embedding visualised in RGB and predicted monocular depth. Without depth estimation, the circled car merges into the red car, while the model with depth does not as there is a significant difference in depth between the two cars.



(a) Without depth estimation.



(b) With depth estimation

Figure 8: From left to right: RGB input image, ground truth instance segmentation, predicted instance segmentation, embedding visualised in 2D, embedding visualised in RGB and predicted monocular depth. The model without depth is not able to handle complete occlusion, while the model with depth can.